Injection Molding of Polypropylene: X-Ray Investigation of the Skin–Core Morphology

W. WENIG* and F. HERZOG

University of Duisburg, Laboratory of Applied Physics, 47048 Duisburg, Germany

SYNOPSIS

The skin–core morphology of injection-molded polypropylene bars has been investigated employing X-ray small- and wide-angle scattering. The small-angle scattering has been evaluated by means of interface distribution functions. It is found that skin and core exhibit different morphologies. In the skin, the crystal lamellae are oriented primarily around the c axis, but a (small) fraction of a^*-axis-oriented lamellae also exists. The lamellar thickness in the skin layer measured from the meridional small-angle X-ray scattering shows higher values than in the core. The composition of the monoclinic α_1, α_2 crystal modifications show dependencies that are typical for the cooling conditions in the mold during injection.

INTRODUCTION

When a polypropylene melt is injected into a mold, a complicated morphology is observed that is often the reason for unfavorable mechanical properties.[1-4] Due to flow and cooling conditions during the injection a sandwich structure ensues that can be roughly separated into three layers[1]: a skin layer, which under the polarization microscope seems to be "structureless," a spherulitic core, and a "transition zone" between these two layers. A number of ingestivations[2-4] showed, that the layer structure is far more complicated and that the skin layer is composed of fibrillar crystals with lamellar overgrowth. The thickness of this layer is controlled by the shear conditions during the mold filling process and varies along the flow path. The crystal orientation and the superstructure of skin and core layers in polypropylene injection-molded parts has been extensively investigated by Clark and Spruiell[5] and by Fujiyama, Wakino, and Kawasaki.[6] Both studies find a bimodal orientation of the unit cell in both the skin and core layer. From small-angle X-ray investigations Fujiyama et al.[6] conclude that the a^*-axis-oriented lamellae are "less perfect" than the c-axis-oriented lamellae and thus do not contribute to interference effects of the small-angle X-ray scattering. This study presents results of small-angle X-ray measurements on skin and core layers of injection-molded isotactic polypropylene parts. The scattering curves are evaluated by means of interface distribution functions.

EXPERIMENTAL

Sample Preparation

Isotactic polypropylene with a molecular weight of M_w = 287,000 was used to produce injection-molded standard tensile bars according to DIN 53455 (length = 150 mm, thickness = 3 mm). The temperature of the melt was 240°C and three sets of samples were prepared using the mold temperatures T_W = 60, 80, and 120°C. To investigate morphological changes as a function of location, from some bars segments were cut out, one segment was taken from the center (segment 2), the other two from both ends of the bar with a distance of 30 mm from the center (segment 1 near the injection gate, segment 3 on the opposite side). From each segment microtome cuts with thicknesses < 150 μm were made and the skin and core pieces were used for the X-ray measurements.

* To whom correspondence should be addressed.

Journal of Applied Polymer Science, Vol. 50, 2163–2171 (1993)
 CCC 0021-8995/93/122163-09

X-ray Experiments

Small-angle X-ray scattering curves were recorded using a Kratky compact camera. The setting of the camera was such that sufficiently high resolution was ensured (entrance slit width = 30 mm, detector slit width = 75 mm, distance sample detector slit = 22 cm). The measurements were controlled by a computer and the temperature of the cooling water was kept constant through a constant-temperature unit. CuKα radiation was used and monochromatization was achieved by using a Ni filter in conjunction with pulse height analysis. Each curve was recorded several times in an angular range corresponding to 0.7×10^{-4} nm $\leq s \leq 40 \times 10^{-4}$ nm ($s = 2 \sin \Theta/\lambda$, 2Θ being the scattering angle and λ the X-ray wave length).

Flat camera exposures were taken using a Philips PW 1012/90 camera. To determine the distance sample to film, A, a KCl powder sample was used. For a known spacing d_{hkl} A is yielded from the equation $2\Theta = \arctan(D/2A)$; $d_{hkl} = \lambda/2 \sin(\Theta)$ where D is the reflection diameter. For all calculations, the following unit cell parameters were employed[7,8]. α modification: $a = 0.663$ nm, $b = 0.2078$ nm, $c = 0.650$ nm, $\beta = 0\ 99°5'$; β modification: $a = 0.1908$ nm, $c = 0.649$ nm. Wide-angle X-ray scattering curves were measured using a Philips PW 1380 Goniometer.

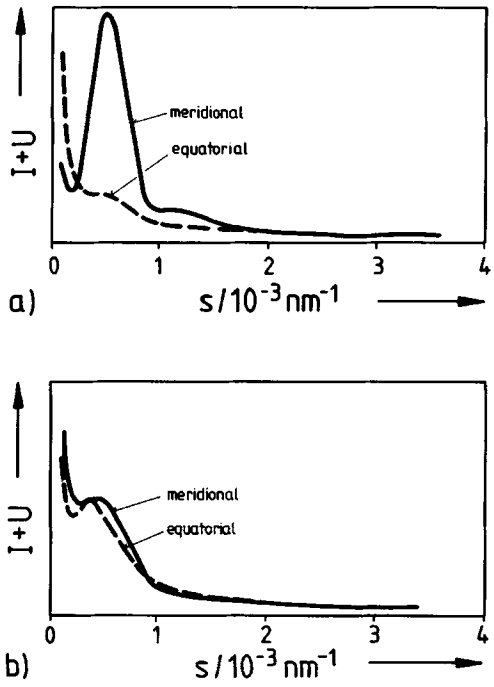

Figure 1 Measured small-angle X-ray scattering curves after smoothing for $T_W = 60°C$, segment 1: (a) skin layer and (b) core.

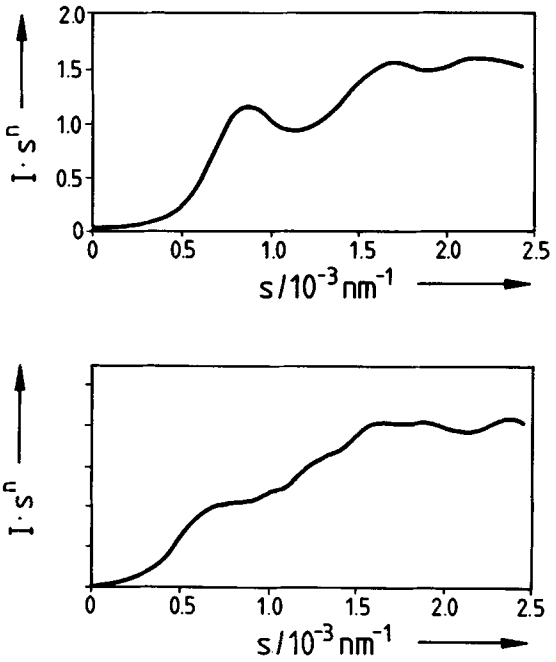

Figure 2 Plot of $Is^n(s)$ of the scattering curves for the skin layer [cf. Fig. 1(a)] after correction for fluctuation scattering.

CuK$_\alpha$ radiation was used and monochromatization was achieved by use of a graphite monochromator. To determine the "order-parameter," the composition of α_1, α_2 monoclinic crystal modification, the angular range $32° \leq 2\Theta \leq 44°$ was measured separately with higher resolution.

The measured small-angle scattering curves have been smoothed[9] and corrected for fluctuation scattering. This fluctuation intensity was assumed to be constant, so that from the measured (slit-smeared) intensity $I_{exp}s^3$ a function Us^3 has to be subtracted. Because for higher s values $I_{exp}s^3$ becomes constant (Porod's law) the fluctuation scattering is subtracted from the measured intensity in such a way, that $I_{corr}s^3$ converges to a constant value:

$$\text{const} = I_{corr}s^3 - Us^3 \tag{1}$$

Using Porod's law, the fit of the fluctuation intensity to $I_{exp}s^3$ has to be done by a vertical shift of the function Us^3:

$$I_{exp}s^3 - Us^3 = K \tag{2}$$

$$U = I_{exp} - K/s^3 \tag{3}$$

Figure 1 shows four measured and smoothed intensity curves taken from skin and core layers at $T_W = 60°C$ (segment 1), and Figure 2 shows the same

curves for the skin (segment 1) after correction for fluctuation scattering.

To obtain intensity values down to $s = 0$, the intensity has to be extrapolated. This can be done by use of Gunier's law:

$$I = I_0 \exp(-\tfrac{4}{3}\pi^2 R_g^2 s^2) \qquad (4)$$

$$\ln I = -\tfrac{4}{3}\pi^2 R_g^2 s^2 + \ln I_0 \qquad (5)$$

where R_g is the radius of gyration. Plotting $\ln I$ versus s (Guinier plot) Eq. (5) is a straight line. The intensity can thus be easily extrapolated, and simultaneously the radius of gyration and the intensity at zero angle can be determined.

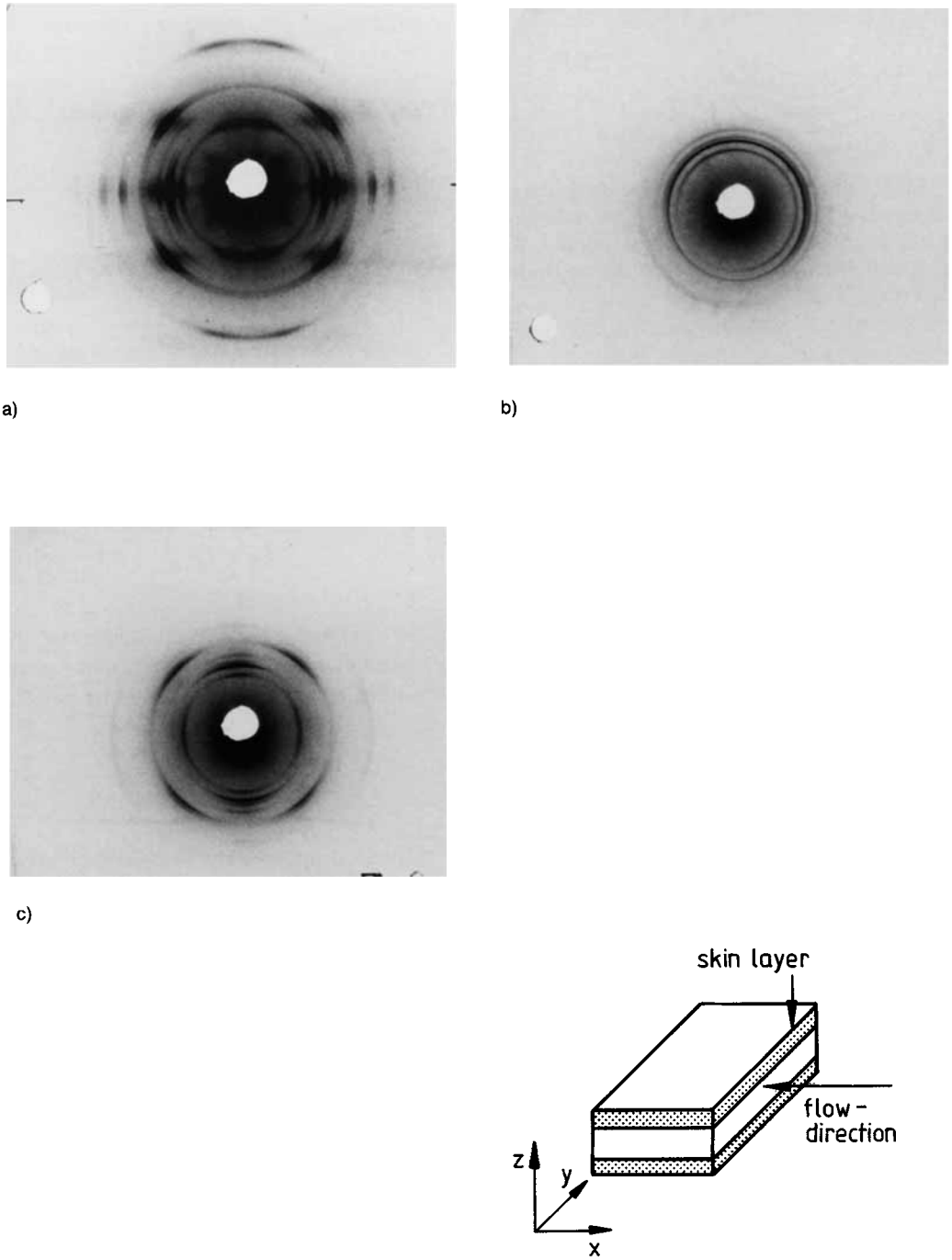

Figure 3 Flat camera exposures of the skin layer for the sample at $T_W = 60°C$, segment 1 in (a) z direction, (b) x direction, (c) y direction.

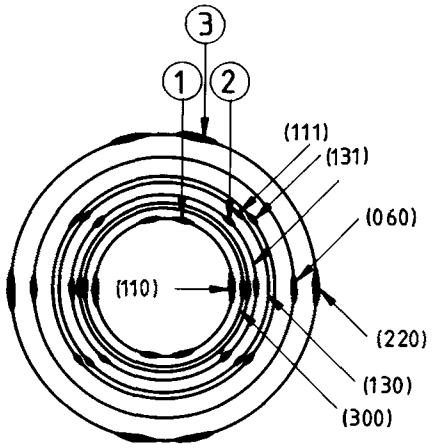

Figure 4 Sketch of the reflections appearing in the exposures displayed in Figure 3. The strongest reflections due to the c-axis-oriented component are indexed. The numbers 1, 2, and 3 mark the reflections due to the a^*-axis-oriented component.

RESULTS

Flat Camera Exposures

Figure 3 shows as an example the flat camera exposures for the skin layer at $T_W = 40°C$ (segment 1). Two types of orientations of the monoclinic crystals can be distinguished. Figure 4 shows a sketch of the reflections that appear in the exposures of Figure 3. The indexed reflections are due to those crystals whose c axis is parallel to the flow direction (x-direction in Fig. 3). The reflexions marked with 1, 2, and 3 can be attributed to crystals whose a^* axis is oriented parallel to the flow direction. This axis is oriented perpendicular to the axes b and c. The reflections 1, 2, and 3 can thus be identified as the (110), (130), and (220) reflections.

Figure 5 displays exposures as a function of distance from the surface, taken in z direction (perpendicular to the flow direction). It is seen that the degree of orientation decreases with distance from the surface. The, however weak, β modification disappears in the core.

Crystal Modification

To determine the α_1, α_2 composition in skin and core layers, the wide-angle scattering in the angular range $32° \leq 2\Theta \leq 44°$ has been measured. Two peaks are measured in this interval: the ($\bar{1}71$), (132), (231), (052) peak (peak 1), and the (171), (241) peak (peak 2).[10,11] While peak 1 contains the contributions of both the α_1 and α_2 modifications, peak 2 is only due to the α_2 modification. An order parameter, R, can be defined by calculating the ratio of the areas under peak 1 to peak 2 (cf. Fig. 6).[11] In Table I the order parameters, R, are listed.

Interface Distribution Functions

For the system given, the one-dimensional intensity $I_1(s)$ of the small-angle X-ray scattering, which is related to the measured intensity $I(s)$ by $I_1(s) \sim s^2 I(s)$ can be calculated from the (linear) Fourier transform of the square of the self-convolution of the electron density distribution[12]

$$I_1(s) = F_1(\Delta\rho_1^{*2}) \quad \text{for } s \neq 0 \tag{6}$$

with

$$\Delta\rho_1 = \rho_1(r) - \langle\rho_1\rangle_t \quad \Delta\rho_1^2 = P_1(r) \tag{7}$$

where $P(r)$ is the correlation function as defined by Vonk and Cortleve.[13]

It further follows that $s^2 I_1(s)$ is proportional to the Fourier transform of the second derivative of the one-dimensional correlation function:

$$-4\pi^2 s^2 I_1(s) = F_1\left(\frac{\partial^2}{\partial r^2} P_1(r)\right) \tag{8}$$

We expand $P(r)$ and introduce the one-dimensional equivalent of Porod's invariant k_1, and the average chord length, d_p, as defined by Ruland[14]:

$$P_1(r) = k_1\left(1 - \frac{|r|}{d_p} + \cdots\right) \tag{9}$$

By decomposing the second derivative of $P_1(r)$ into a delta function at the origin ($r = 0$) and a function $g_1(r)$ for $r \neq 0$, we get

$$\frac{\partial^2}{\partial r^2} P_1(r) = -\frac{2k_1}{d_p}\delta(r) + g_1(r) \tag{10}$$

where $g_1(r)$ is the interface distribution function.[12]

Using Eq. (10), Eq. (8) then becomes

$$4\pi^2 s^2 I_1(s) = \frac{2k_1}{d_p} - G_1(s) \tag{11}$$

where $G(s)$ is the interference function connected with the interface distribution function by a one-dimensional Fourier transform:

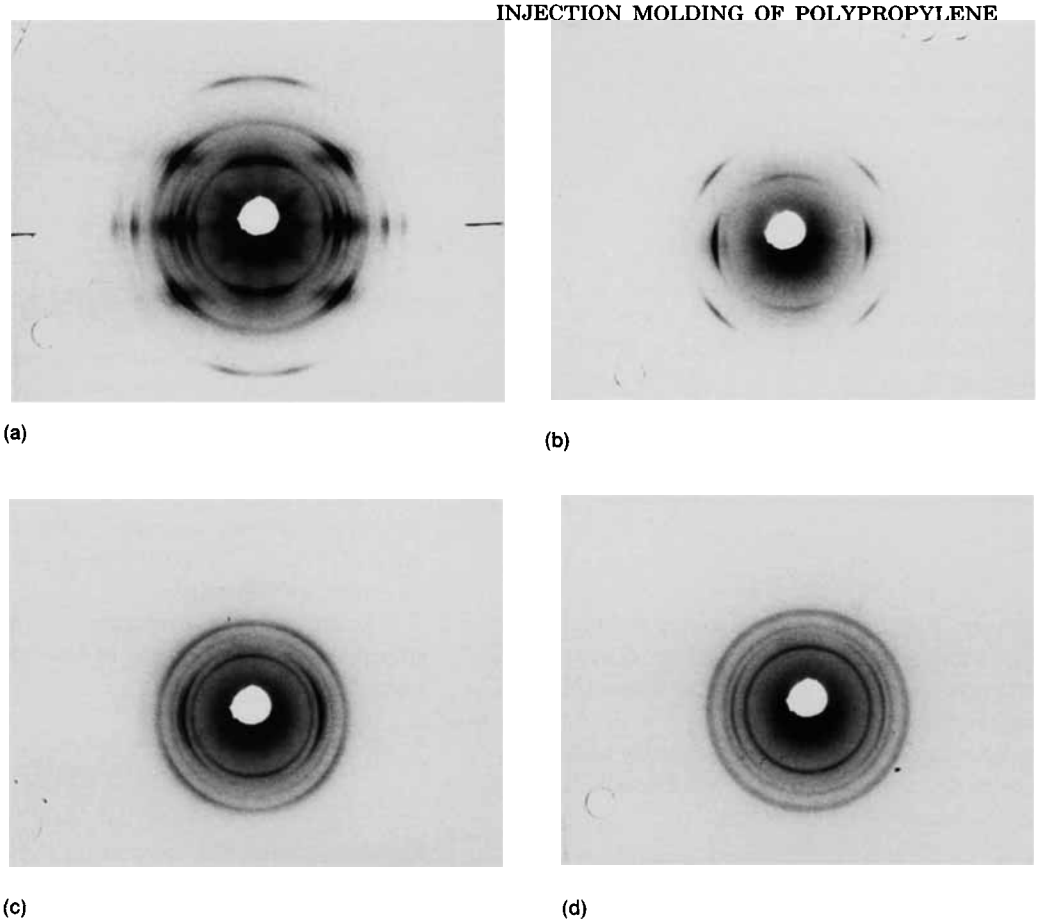

Figure 5 Flat camera exposures taken in various depths in the sample (T_W = 60°C, segment 1): (a) skin, specimen thickness: 150 μm; (b) depth: 185 μm, spec. thickness: 65 μm; (c) depth: 340 μm, spec. thickness: 85 μm; (d) depth: 750 μm, spec. thickness: 80 μm.

$$G_1(s) = F_1[g_1(r)] \qquad (12)$$

$$g_1(r) = F^{-1}[G_1(s)] \qquad (13)$$

$g_1(r)$ therefore calculates from $G(s)$ by an inverse Fourier transform:

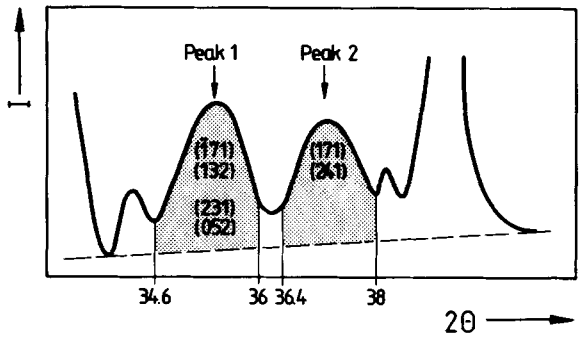

Figure 6 Determinations of the order parameter R of α_1, α_2 crystal modifications. R is defined as the ratio of the area under peak 1 to peak 2,[10] peak 1 is generated by contributions from both the α_1 and α_2 modifications and contains indices $h + k$ even and odd, while peak 2 is only due to the (lower ordered) α_1 modification with only even indices.

To evaluate $G_1(s)$ from the scattered intensity, the influence of the interface between crystals and the amorphous environment has to be corrected. Ruland[14,15] as well as Koberstein, Morra, and Stein[16,17] assume a Gaussian-shaped transition of the electron density created by the Fourier transform of the first derivative of the electron density (which yields positive and negative Gauss peaks on both sides of the crystal):

$$I_{\text{gauss}} = C \exp(-a \cdot s^p) \quad C, a > 0 \qquad (14)$$

Table I Order Parameters

	Skin			Core		
Segment	60°C	80°C	120°C	60°C	80°C	120°C
1	0.28	0.58	0.79	0.66	0.74	1.39
2	0.32	0.37	0.74	0.54	0.62	0.97
3	0.35	0.40	0.63	0.41	0.49	0.83

with $p = 1.81$ for slit-smeared curves[17] and $p = 2$ for unsmeared curves.[15] a is calculated from

$$a = \left(\frac{2\pi\, d_z}{3}\right)^2 \tag{15}$$

where d_z is the length of the interface. d_z can be approximated by $d_z \sim 3\xi$, with ξ = standard deviation of the electron density variation and C is obtained from:[18]

$$C = \frac{\int_{s_1}^{s_{max}} Is^n\, ds}{\int_{s_1}^{s_{max}} \exp(-as^p)\, ds} \tag{16}$$

C is determined by fitting the curve defined by eq. (14) in such a way that in the Porod part of the curve (beginning at $s = s_1$) the areas under this curve and the curve $Is^n(s)$ are equal.[18]

Because the decrease of the intensity at high s is a measure for the deviation from Porod's law, the "compensation" of the decrease

$$Is^n = C \exp(-as^p) \tag{17}$$

yields the interface length. A plot of $\ln(Is^3)$ versus $s^{1.81}$ (Koberstein–Morra–Stein plot) is shown in Figure 7.

As a result, we obtain the "interface corrected" intensity from which the interference function is calculated. This function is determined by

$$G_1(s) = \frac{16\pi^2 t}{V}\left[C - D\exp(-As^2) - Is^n\right] \tag{18}$$

with V the scattering volume and t the average stack height of lamellar stacks. C, D, and A are parameters that have to be determined by fitting a base-function (proportional to the gas scattering of the corresponding system showing only particle scattering) (cf. Fig. 8).[18] Figure 9 shows an example for the interference function.

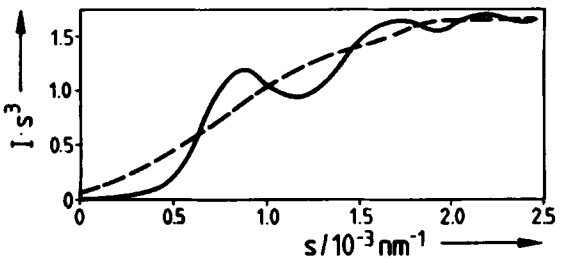

Figure 8 Interface corrected intensity $Is^3(s)$ of the meridional scattering of the skin layer (T_W = 60°C, segment 1). A base function is fitted into the curve to evaluate the interference function.

The interface distribution function is then calculated by the transform of the interference function:

$$g_1(r) = \int_0^\infty G_1(s)\cos(2\pi rs)\, ds \tag{19}$$

Figure 10 shows the interface distribution functions for the samples at T_W = 60°C, segment 1. We see that the values for interlamellar distance, lamellar thickness, and long period can be well resolved. The results are listed in Table I.

DISCUSSION

The results allow a discussion of the structural models proposed by Clark and Spruiell[5] and by Fujiyama, Wakino, and Kawasaki.[6] Both studies find that in the textured skin layer the c and a^* axes are oriented in flow direction. The crystal lamellae, whose average thickness amount to 16 nm, are oriented normal to this direction. Fujiyama et al.[6] calculated orientation functions. It is found that f_c is

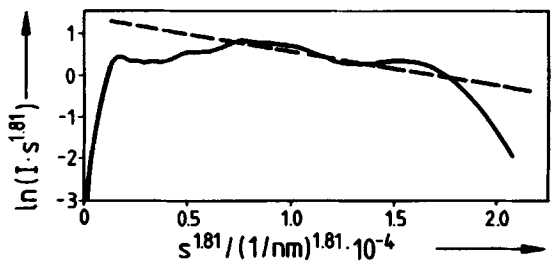

Figure 7 Koberstein–Morra–Stein plot of the meridional scattering of the skin layer (T_W = 60°C, segment 1).

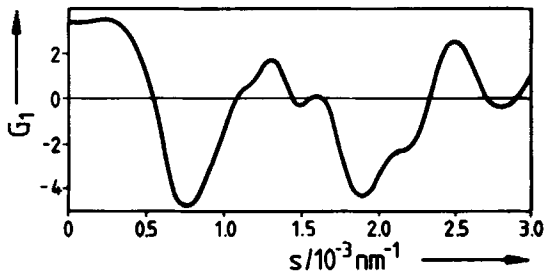

Figure 9 Interference function calculated from the curve displayed in Figure 8.

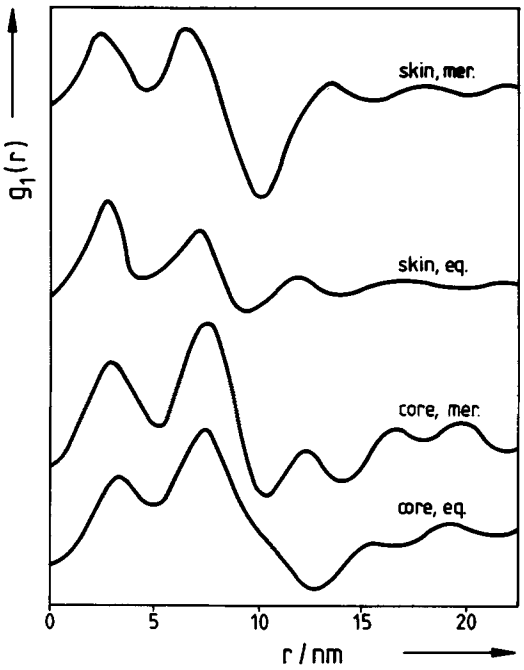

Figure 10 Interface distribution functions of the samples at $T_W = 60°C$, segment 1.

positive, f_b and f_a^* negative. An orientation in flow direction of the melt should, however, give positive values for f_b and f_a^*. Fujiyama et al. explain this as follows: when c-axis-oriented and a^*-axis-oriented components coexist, the a^* axis of the c-axis-oriented component and the c axis of the a^*-axis-oriented component are perpendicular to the flow direction. Therefore, on calculating orientation functions, the c axis of the c-axis-oriented component and the c axis of the a^*-axis-oriented component contradict each other, and the same holds for the a^* axis with respect to the c axis and a^* axis orientation, respectively. If, as we also find in our experiments, the orientation functions have different amounts, then the signs of the functions f_c and f_a^* are determined by a balance of the amount and orientation degree of the c- and a^*-axis components.[6] This means that for the samples investigated in this work, the orientation of the c-axis component is higher than that of the a^*-axis component.

As we learn from the flat camera exposures, the amounts of the orientation functions of the core are obviously smaller. Therefore, the crystal lamellae in the core seem to be unoriented. On the other hand, the azimuthal intensity distribution of the (110) peaks show that f_c must be positive. Therefore, also in the core a c-axis orientation must exist. Clark[5,19] discusses a two-stage crystallization process as a result of the cooling conditions in the mold. In the first stage, a row structure of planar lamellae are built, which crystallize from fibrillar nuclei. The growth axis of these lamellae is parallel to the a^* axis. Under the assumption of regular folding, the fold surface is the (110) plane. In the second stage, a portion of the molecules is rejected from the growing lamellae into the interlamellar space where it crystallizes a short time later (interlamellar transcrystallization). A special type of epitaxial crystallization (between the folds on the primary lamellae) causes the orientation of the chain axes of the secondary component to be perpendicular to the chain axes of the primary component. Consequently, the a^* axis of the secondary component should be oriented perpendicular to the c axis of the primary crystals, which is, as we see from the results, indeed the case.

The small-angle X-ray patterns measured by Fujiyama et al.[6] show for the skin layer an orientation in meridional direction. The patterns show no modulation of the equatorial scattering, which however, should occur, if an a^*-axis orientation is present. The authors conclude from their findings that a^*-direction-oriented lamellae are less perfect (high fluctuations of thickness and distance distributions). In the core an interparticulate interference is measured in both meridional and equatorial direction.

Our measurements yield a modulation of the small-angle scattering (maxima or shoulders) for all curves (e.g., in the skin layer for both meridional and equatorial scattering cf. Fig. 1). This can be interpreted as follows: The contribution to the equatorial scattering maximum of the skin layer can be attributed either to the a^*-axis orientation (where the lamella normals are oriented in equatorial direction) or to a fluctuation of the lamella orientations around the c axis. An answer is given by comparing the meridional and equatorial scattering of the core: The orientation of the c axes is here approximately statistical, only a very weak orientation can be measured. The equatorial scattering should therefore exhibit a somewhat less pronounced maximum than the meridional scattering and should have (in the region of the maximum) an intensity below that of the meridional scattering curve. An additional a^*-axis orientation should provide an additional contribution to the scattered intensity in this angular range. The maximum of the equatorial scattering should therefore have a higher intensity than the meridional scattering. Our measurements show, however, that the intensity of the equatorial scattering is always below that of the meridional scattering (cf. Fig. 1). We can therefore conclude

that the crystal lamellae in the skin layer are oriented around the c axis.

Another interesting result is yielded from the calculation of the invariants.

$$Q = \int_0^{s_{max}} sI(s)\, ds \qquad (20)$$

For T_W = 60°C and segment 1, we find for Q the values 5.92 (meridional scattering) and 3.46 (equatorial) for the skin, and 9.79 (meridional) and 9.27 (equatorial) for the core. At T_W = 120°C, segment 1, similar values are found except for the meridional scattering of the skin layer: skin 11.64 (meridional) and 5.64 (equatorial), core 9.14 (meridional) and 9.19 (equatorial). We thus find that in the skin layer the invariants of the meridional scattering are higher than those of the equatorial scattering, while for the core the values for Q are similar. This means that in the skin layer the crystallinity is considerably smaller in equatorial direction than in meridional direction. It also shows that the scattering in the skin layer is generated primarily by those lamellae that are oriented in c direction and that the fraction of a^*-axis-oriented lamellae is small.

The morphological parameters (lamellar thicknesses, interlamellar distances, and long periods) show for the meridional direction higher values in the skin layer than in the core (cf. Table II) while for the equatorial direction similar values are found. This can hardly be explained by a uniform morphology in both core and skin layer but may indicate the presence of "shish-kebabs" in the skin as has been proposed by Clark and Spruiell[5] and by Fujiyama et al.[6] An a^*-axis-oriented component in the skin layer should, however, display a morphology that is likely to be similar to that in the core. Considering the relatively low value of the invariant for the equatorial scattering of the skin layer, the contribution of the fraction of a^*-axis-oriented lamellae is obviously small. This explains the differences of the values of the invariants and the results of the interface distribution function calculations.

We see that the morphology of the samples is strongly influenced by the shear forces during the injection of the melt. Other parameters, like the mold temperature, are of minor influence. Lamellar thickness, interlamellar distance, and long period vary only slightly with mold temperature and location (segment); obviously they are only influenced by the cooling conditions during injection of the melt.

The order parameter, R, designating the composition of α_1, α_2 crystal modifications, appears higher in the core than in the skin. This is obviously due to slower cooling of the polypropylene melt in the core, since a higher R value means a higher "order" of the monoclinic crystal structure.[10,11] Consequently, the R value increases with the mold temperature because the temperature difference between melt and mold is smaller at higher T_W. Order parameter R also increases slightly with distance from the injection gate (segment). This can be understood from two reasons: The temperature of the melt decreases while flowing through the mold, and the shear forces near the wall decrease toward the end of the mold. Consequently, the order parameter increases. Concurrently, the crystallinity is found to decrease from segment 1 to segment 3 (cf. Fig. 11). That the shear forces have an influence on the crystallinity is shown by the increase of X_c from core to skin.[20–22] Also for higher mold temperatures the crystallinity increases due to the lower temperature difference.

Table II Results from Interface Distribution Function Calculations[a]

			Skin		Core	
	T_w		Merid.	Equat.	Merid.	Equat.
d_c	60°C	Seg. 1	9.0	7.4	7.5	8.1
		Seg. 2	7.5	9.1	7.6	7.5
	80°C	Seg. 1	8.3	7.5	8.0	8.5
	120°C	Seg. 1	10.6	10.7	7.2	10.3
		Seg. 2	10	7.4	7.5	8.4
		Seg. 3	11.6	7.5	8.1	7.6
d_a	60°C	Seg. 1	3.1	2.1	3.8	1.8
		Seg. 2	4.3	1.7	2.7	2.6
	80°C	Seg. 1	4.1	2.4	5.1	3.6
	120°C	Seg. 1	3.6	2.0	2.5	2.1
		Seg. 2	5.8	1.9	2.9	2.4
		Seg. 3	3.4	2.5	2.1	3.0
L	60°C	Seg. 1	12.1	9.7	11.2	10.3
		Seg. 2	11.9	11.1	10.4	10.1
	80°C	Seg. 1	12.4	10.8	13.2	11.9
	120°C	Seg. 1	14.3	12.9	9.9	12.6
		Seg. 2	15.6	9.6	10.5	11.2
		Seg. 3	15.0	10.2	10.2	10.6

[a] T_w, mold temperature; d_c, mean lamellar thickness; d_a, mean interlamellar thickness, L, long period. All numbers in nanometers.

CONCLUSIONS

1. Skin and core layers in injection-molded polypropylene contain different morpholo-

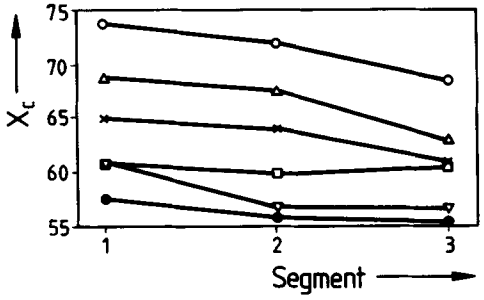

Figure 11 Crystallinity as a function of sample segment

gies. While in the core an almost unoriented spherulitic morphology exists, the skin exhibits an oriented "shish-kebab"-type structure.

2. Responsible for the skin structure are the shear forces occurring during the injection of the melt. These shear forces, however, are not so high as to induce complete fibrillar crystallization: while most of the crystal lamellae are oriented around the c axis, there still exists a (smaller) fraction of a^*-axis-oriented lamellae.
3. The lamellar morphology in both core and skin layer is influenced by the temperature of the mold. The changes of the morphological parameters, like lamellar thickness and interlamellar distance, can be explained by the cooling conditions of the melt during injection.
4. The order parameter R designating the composition of the monoclinic α_1, α_2 modifications, shows characteristic dependencies: The order is higher in the core than in the skin, and R increases with mold temperature. Also, near the gate of the mold, R has a lower value than on the opposite side. These dependencies can all be explained by the cooling conditions in the mold, since they are in good accordance with the known annealing behavior of R.

REFERENCES

1. M. R. Kantz, H. D. Newman, and F. H. Stigale, *J. Appl. Polym. Sci.*, **16,** 1249 (1972).
2. F. Altendorfer and E. Seitl, *Kunststoffe,* **76,** 47 (1986).
3. G. Menges, G. Wübken, and B. Horn, *Coll. Polym. Sci.*, **254,** 267 (1976).
4. J. P. Trotignon, J. L. Lebrun, and J. Verdu, *Plast. Rubber Proc. Appl.*, **2,** 247 (1982).
5. E. S. Clark and J. E. Spruiell, *Polym. Eng. Sci.*, **16,** 176 (1976).
6. M. Fujiyama, T. Wakino, and Y. Kawasaki, *J. Appl. Polym. Sci.*, **35,** 29 (1988).
7. Z. Mencik, *J. Macromol. Sci. Phys.*, **6,** 101 (1972).
8. L. G. Berry, Ed., *Powder Diffraction File,* JCPDS, Philadelphia, 1974.
9. H. W. Fiedel, T. Schöller, J. Petermann, and W. Wenig, *Coll. Polym. Sci.*, **264,** 1017 (1986).
10. G. Guerra, V. Petraccone, P. Corradini, C. DeRosa, and R. Napolitano, *J. Polym. Sci., Polym. Phys. Ed.*, **22,** 1029 (1984).
11. C. DeRosa, G. Guerra, R. Napolitano, V. Petraccone, and B. Pirozzi, *Eur. Polym. J.*, **20,** 937 (1984).
12. W. Ruland, *Coll. Polym. Sci.*, **255,** 417 (1977).
13. C. G. Vonk and G. Kortleve, *Koll. Z. Z. Polym.*, **220,** 19 (1967).
14. W. Ruland, *Coll. Polym. Sci.*, **256,** 932 (1978).
15. M. Stribeck and W. Ruland, *J. Appl. Cryst.*, **11,** 535 (1978).
16. J. T. Koberstein, B. Morra, and R. S. Stein, *J. Appl. Cryst.*, **13,** 34 (1980).
17. J. T. Koberstein and R. S. Stein, *J. Polym. Sci., Polym. Phys. Ed.*, **21,** 2181 (1983).
18. H. W. Fiedel and W. Wenig, *Coll. Polym. Sci.*, **267,** 389 (1989).
19. E. S. Clark, *Bull. Am. Phys. Soc.* (1970).
20. S. Katti and J. M. Shultz, *Polym. Eng. Sci.*, **22,** 16 (1982).
21. G. Menges, H. Ries, and T. Wiegmann, *Kunststoffe,* **77,** 433 (1987).
22. K. Pleßmann, G. Menges, M. Cremer, W. Fenske, W. Feser, C. Netze, H. Offergeld, G. Pötsch, and H. Stabrey, *Kunststoffe,* **80,** 200 (1990).

Received April 5, 1993
Accepted June 9, 1993